Environmental Science & Technology

pubs.acs.org/est

Article

Uptake and Toxicity of Respirable Carbon-Rich Uranium-Bearing Particles: Insights into the Role of Particulates in Uranium Toxicity

Eliane El Hayek,* Sebastian Medina, Jimin Guo, Achraf Noureddine, Katherine E. Zychowski, Russell Hunter, Carmen A. Velasco, Marco Wiesse, Angelea Maestas-Olguin, C. Jeffrey Brinker, Adrian Brearley, Michael Spilde, Tamara Howard, Fredine T. Lauer, Guy Herbert, Abdul Mehdi Ali, Scott Burchiel, Matthew J. Campen, and José M. Cerrato

Cite This: *Environ. Sci. Technol.* 2021, 55, 9949−9957

Read Online

ACCESS | Metrics & More | Article Recommendations | Supporting Information

ABSTRACT: Particulate matter (PM) presents an environmental health risk for communities residing close to uranium (U) mine sites. However, the role of the particulate form of U on its cellular toxicity is still poorly understood. Here, we investigated the cellular uptake and toxicity of C-rich U-bearing particles as a model organic particulate containing uranyl citrate over a range of environmentally relevant concentrations of U (0−445 μM). The cytotoxicity of C-rich U-bearing particles in human epithelial cells (A549) was U-dose-dependent. No cytotoxic effects were detected with soluble U doses. Carbon-rich U-bearing particles with a wide size distribution (<10 μm) presented 2.7 times higher U uptake into cells than the particles with a narrow size distribution (<1 μm) at 100 μM U concentration. TEM-EDS analysis identified the intracellular translocation of clusters of C-rich U-bearing particles. The accumulation of C-rich U-bearing particles induced DNA damage and cytotoxicity as indicated by the increased phosphorylation of the histone H2AX and cell death, respectively. These findings reveal the toxicity of the particulate form of U under environmentally relevant heterogeneous size distributions. Our study opens new avenues for future investigations on the health impacts resulting from environmental exposures to the particulate form of U near mine sites.

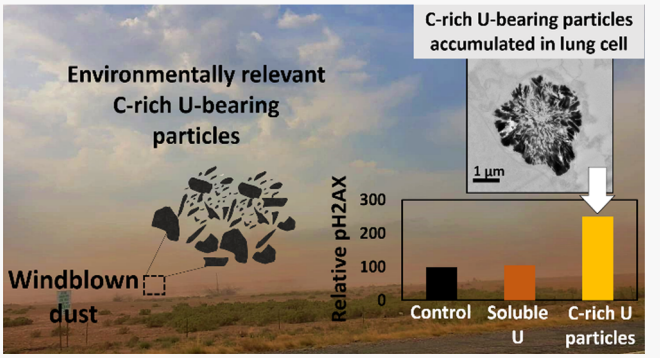

KEYWORDS: *windblown dust, inhalation, bioaccumulation, cytotoxicity, genotoxicity, health risks*

INTRODUCTION

The inhalation of respirable particulate matter (PM) is considered one of the top global health risks for cardiorespiratory mortality and morbidity by the World Health Organization and the Global Burden of Disease project.[1] Populations, such as the many indigenous communities in the southwestern United States, reside in close proximity to mine waste sites and, as a result, are at especially high risk of heavy metal-rich PM exposure.[2−5] Documented health hazards in communities located close to mine sites include hypertension and cardiovascular and kidney diseases, all of which are associated with metal-bearing PM exposure.[2,6] Recent findings in a Navajo population indicate that residential proximity to abandoned uranium (U) mine sites results in increased serum inflammatory potential.[7] However, associations between inflammation and ingested metals were not detected, suggesting that inhalation may represent a critical, but understudied factor in these populations.[7]

Legacy U mine sites in semi-arid regions are subject to strong eolian processes, which enhance the dispersion and air transport of U-bearing mineral dust, causing concern for toxicological effects on health.[8] Recent studies at the Jackpile Mine located on the Pueblo of Laguna, New Mexico, highlight the role of windblown dust transport in the release of U into the environment.[3,9] Fine-grained, U-bearing particulates occur in a variety of mineral associations, including with natural organic matter (NOM).[10−12] An important chemical characteristic of the mineralized deposits from the mine sites in New Mexico is the encapsulation of concentrated U by high NOM content [13−44% carbon(C) by weight].[12−14] To date, the health risks related to suspended PM arising from legacy mine sites are not well defined, and the toxicity of U-bearing particulates remains underestimated.

Received: February 21, 2021
Revised: June 30, 2021
Accepted: July 1, 2021
Published: July 8, 2021

Inhalation of U is one of the most significant exposure pathways.[15] Epidemiological studies highlight the risk of developing lung cancer and chronic respiratory diseases following exposure to U dusts.[7] In rat broncho-alveolar lavage cells, inhalation of U oxide induced DNA damage and oxidative stress.[16] A recent study demonstrated that mine site-derived PM (Blue Gap Tachee, AZ), containing U, vanadium (V), and other metals, induces greater pulmonary inflammation than regional background PM.[2] Mine-site-derived PM from Blue Gap Tachee, AZ, and that from St. Anthony mine, NM, were also detected to induce neurological and pulmonary inflammatory effects.[17] However, the aforementioned studies focused on solid mineral PM containing metal mixtures and did not specifically discriminate the role of the particulate forms in the lung environment, as compared to the dissolved forms of metals. Dissolved and particulate forms of metals can induce distinguished mechanisms of cellular toxicity. In the case of U, most in vitro and in vivo toxicity studies use only soluble U (e.g., U salts such as uranyl acetate),[15,18] leaving critical knowledge gaps regarding the interaction of the particulate form of U within cellular compartments. Factors such as the size, composition, and source of particulates affect the mechanisms of cellular toxicity.[19,20] Understanding these mechanisms is important to identify the health risks in affected communities.

The objective of this study is to determine the cellular uptake and toxicity of respirable synthesized C-rich U-bearing particles as a model organic particulate over a range of environmentally relevant U concentrations (0−445 μM).[21−23] Carbon-rich U-bearing particles are used in this study as a solid particulate phase of U distinct from soluble U salts that have been used for other toxicity studies.[2,24,25] We investigated the effects of different size distributions of C-rich U-bearing particles on cell viability, genotoxicity, intracellular U concentration, and the translocation of particles into the human lung epithelial cell model (A549). The cytotoxicity of particulate U was emphasized by using organosilica particles containing comparable organic content but without U and silica particles as an additional control. A novel aspect of this study pertains to the effects of the particulate form of U and the size of the particles on U intracellular bioaccumulation and toxicity, as compared to the soluble U form. This information is relevant to understanding the environmental health risk exposures to U particulates derived from mine wastes, mill tailings, nuclear power plants, and other industrial settings.

MATERIALS AND METHODS

Preparation and Characterization of C-Rich U-Bearing Particles. Carbon-rich U-bearing particles were synthesized according to a method from Thuéry (2006) by combining uranyl nitrate $UO_2(NO_3)_2.6H_2O$ (200 mg, 0.4 mmol) with citric acid (77 mg, 0.4 mmol) in 4.2 mL of ultrapure water containing 800 μL of NaOH (1 M, 0.8 mmol).[26] Citrate was selected to precipitate U in a model organic particulate as it is a known environmentally relevant complexing agent of U, affecting both U solubility and mobility.[26−28] The synthesis was conducted at 180 °C for 48 h. The precipitate was then collected, washed three times with ultrapure water, and finally centrifuged at different speeds in sterile ultrapure water to split the synthesized particles into different size groups. The synthesized C-rich U-bearing particles were evaluated in this study in two environmentally relevant size distributions. One group had wide size distributions (WS, <10 μm) comparable in heterogeneity to PM_{10}. The second group had a narrow size distribution (NS, <1 μm) comparable to PM_1. The size, chemical composition, and crystallinity of particles were studied using scanning electron microscopy (SEM), electron microprobe analysis, high-resolution transmission electron microscopy, and electron diffraction analyses. Inductively coupled plasma-optical emission spectrometry (ICP-OES) was used to determine the concentration of U in the WS and NS suspensions from which serial dilutions were prepared for cell exposure experiments. Detailed information on C-rich U-bearing particle suspensions and their solid characterization is provided in the Supporting Information.

Synthesis of Organosilica and Silica Particles. Siliceous particle synthesis was adapted from literature techniques; particles were made according to a surfactant-templated sol−gel process.[29,30] Briefly, a soluble silica or organosilica source (tetraethylorthosilicate or 1,2-bis(triethoxysilyl)ethylene, respectively) underwent a series of hydrolysis-condensation reactions, under basic conditions (pH = 11) in the presence of cetyl ammonium bromide (CTAB) to yield CTAB-templated particles. The removal of the surfactant occurred by electrostatic exchange of the positive CTAB with protons of acidic ethanol. The full synthesis procedure can be found in the Supporting Information.

Cell Culture. Human adenocarcinoma lung epithelial cells (A549, ATCC) were used to study the interaction of C-rich U-bearing particles in the lungs. The A549 cell model is commonly used to investigate the cytotoxicity and the uptake of particulates with respect to specific particle characteristics.[31−34] Measurements were run in triplicate for each sample in all experiments. Control cells were cultured with an F-12 k regular culture medium without soluble U or particles as a negative control, while cells cultured with etoposide (cytotoxic agent) at a concentration of 200 μM served as a positive control for toxicity bioassays. More information on cell culture is provided in the Supporting Information.

Cell Viability and Genotoxicity Assays. The cell viability of A549 was assessed using the CellTiter-Blue Cell Viability Assay (Promega Corporation, evaluates the metabolic activity of cells). Dose−response was tested following treatments with C-rich U-bearing particle suspensions or the molar equivalent of soluble U solutions at environmentally relevant concentrations of U (from 0.01 to 445 μM).[13,23] The effects of the U particulate form on cell viability were emphasized by comparing C-rich U-bearing particles to organosilica particles containing comparable organic content without U and pure silica particles as an additional control. As a secondary measure of cytotoxicity, cell death was assessed by propidium iodide staining that tests membrane permeability. DNA damage was measured in A549 cells by examining H2AX phosphorylation (pH2AX) using the Invitrogen High Content Screening (HCS) DNA damage kit (Catalog no. H10292). To assess whether C-rich U-bearing particles and soluble U interact with the cell membrane, we assessed the dose-dependent lysis of red blood cells (RBCs). Comparisons between untreated (control) and exposed groups (particles suspensions or soluble U) were performed using a one-way analysis of variance (ANOVA) and Dunnett's t-test at a significance level of $p < 0.05$. More information on cell preparation, exposure, and statistical analyses is provided in the Supporting Information.

Cellular Uptake and Particle Translocation. Total U in acid-digested cell pellets was measured using inductively

https://doi.org/10.1021/acs.est.1c01205
Environ. Sci. Technol. 2021, 55, 9949−9957

coupled-plasma mass spectrometry (ICP-MS) (PerkinElmer NexION 300D), following the exposure of A549 cells to C-rich U-bearing particles and soluble U at 10 and 100 μM U concentrations for 0.5, 1, 2, and 24 h. The intracellular uptake of particles was determined using transmission electron microscopy energy-dispersive spectroscopy (TEM-EDS). Additional descriptions of sample preparation and the methods used are presented in the Supporting Information.

RESULTS AND DISCUSSION

Characterization of C-Rich U-Bearing Particles. Carbon-rich U-bearing particles exhibited a crystalline structure and composition of U, C, H, and O with an average weight percentage of U (59 ± 5%) and C (22 ± 5%), as determined by electron diffraction and SEM-EDS analyses, respectively (Figure 1 and Figure S1). Uranium and C were homogeneously distributed throughout the particles as shown by microprobe analysis (Figure S1). The NS particles presented a narrow distribution of particle size and shape presenting lengths ranging from <0.2 to 0.85 μm (Figure 1A,C); and the WS appeared as polydisperse particles with a wide size and shape distribution (Figure 1B,C and Figure S1) presenting lengths ranging from <0.2 to 10 μm. The rationale for this study was to evaluate the size−uptake−toxicity relationship in lung epithelial cells between the WS (comparable to PM_{10}) and the NS particles (comparable to PM_1). The concentration of U measured in the acid-digested suspensions of particles by ICP-OES was 74.6 ± 0.7 μg of U per 100 μg of particles for the WS and 53.3 ± 0.7 μg of U per 100 μg of particles for the NS. The zeta potential of particles in aqueous suspensions was negative for both WS (−40 ± 0.5 mV) and NS particles (−25 ± 0.3 mV) (Figure 1D).

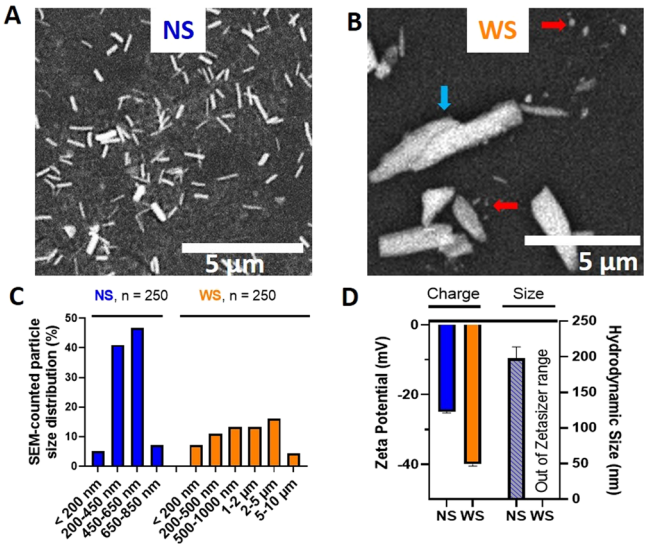

Figure 1. SEM images of (A) NS and (B) WS groups of C-rich U-bearing particles. Light blue and red arrows point to large and smaller particles, respectively. (C) SEM-counted particle size distribution (n = 250). (D) Zeta potential and hydrodynamic size of NS and WS groups of C-rich U-bearing particles.

The aqueous dispersion of NS particles showed an average hydrodynamic diameter of 198 ± 16 nm (Figure 1D). Due to the limitations of this method, dynamic light scattering (DLS) measurements were only applicable to the NS particles, as this measurement is considered accurate for particles with a hydrodynamic diameter less than 1 μm. DLS detected the relative stability of NS particles in cell culture media (F-12K) and in HEPES buffer during the entire experimental period (48 h) with average hydrodynamic diameters of 159 ± 5 and 353 ± 25 nm, respectively (Figure S2). The decreased hydrodynamic diameter averages in cell culture media can be attributed to the protein corona, which causes a change in the refractive index. Particle stability was further supported by TEM images showing no detectable deterioration of the particles (Figure S2). Also, notably the PBS buffer induced a spontaneous strong aggregation, most likely due to the interaction between U with phosphate groups. To prevent particle aggregation during cell exposure experiments, HEPES buffer was selected as a washing solution instead of PBS.

Viability of Cells Exposed to C-Rich U-Bearing Particles. Exposure to WS or NS C-rich U-bearing particles significantly decreased cell viability ($p < 0.05$) in A549 cells in comparison with cells exposed to soluble U (Figure 2A and Figure S3). Cytotoxicity studies were carried out following 24 and 48 h exposure to C-rich U-bearing particles (WS and NS) at U concentrations ranging from 0.01 to 445 μM. These U concentrations are equivalent to 0.0032−143 μg of particles per mL for the WS group and 0.0045−200 μg of particles per mL for the NS group (Tables S1 and S2). Both WS and NS induced a similar cytotoxicity pattern, reaching ∼40% cell death at low U-equivalent concentrations (10 μM) and between 60−90% cell death at higher U concentrations (100−445 μM) at 48 h exposure (Figure 2A). Interestingly, cells treated with soluble U (U aq) at the same molar equivalent (and cells treated with soluble citrate as the additional control) did not show any significant toxicity, with less than 10% cell death at the highest concentration (445 μM U) throughout the exposure duration (Figure 2A). Notably, the WS and NS cytotoxicity pattern was dictated by U doses, rather than the mass concentration of particles (Tables S1 and S2), which supports a U-dose-dependent toxicity. Additionally, in order to evaluate the input of C in the cell toxicity, we compared the toxicity (Figure 2B,C) of C-rich U-bearing particles to organosilica containing 18% organic content by weight, which fits in the range of %C of C-rich U-bearing particles but also exhibiting the same range of negative charge and particle shape heterogeneity (Figure S4). Pure silica particles were used as the secondary control for both C-rich U-bearing particles and organosilica, as exposure to the purely mineral particulate counterparts is postulated to cause silicosis.[35] Carbon-rich U-bearing particles were 1.5 to 4-fold more toxic than organosilica and silica particles, suggesting that the chemical composition of C-rich U-bearing particles, particularly U, plays a key role in inducing cytotoxicity. Moreover, the negligible toxicity produced by soluble U and soluble citrate (both components make the skeleton of the synthesized C-rich U-bearing particles) suggests that U under the organic particulate form has a seminal effect in the induction of cellular toxicity. These results were confirmed by propidium iodide staining, which showed a U-dose-dependent toxic effect of particles on cell death, with the WS particles showing a moderately higher toxicity than the NS particles after 24 h treatment (Figure 2D).

In this study, the toxicity of U was only detected in the presence of C-rich U-bearing particles, which played the role of a vector for U toxicity in lung cells. The negligible toxicity with soluble U treatment suggests that the toxic effects observed with the particles are likely related to the particulate interaction

https://doi.org/10.1021/acs.est.1c01205
Environ. Sci. Technol. 2021, 55, 9949−9957

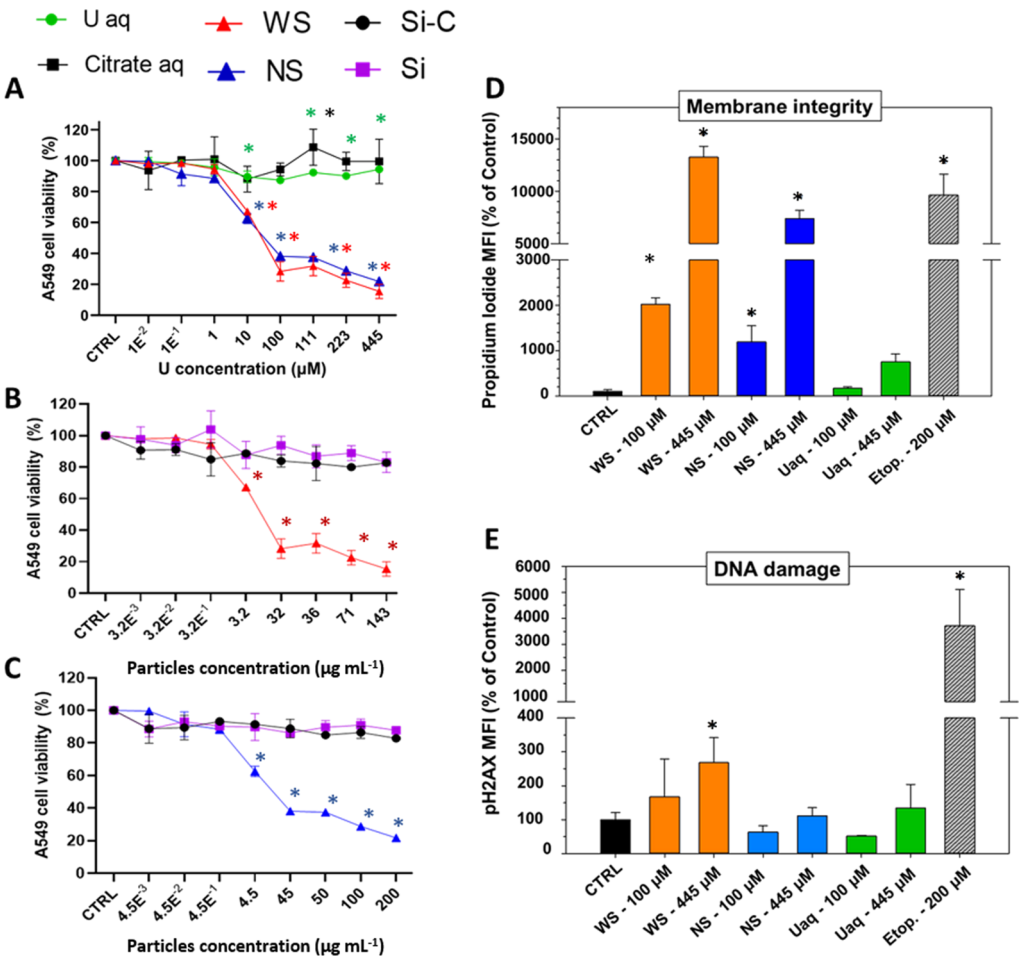

Figure 2. (A) A549 cell viability (%) following exposure to WS and NS groups of C-rich U-bearing particles, soluble U (U aq), and soluble citrate (citrate aq). Comparison of cell viability (%) for cells exposed to (B) WS particles and (C) NS particles with silica and organosilica particles. (D) Cell death measured by mean fluorescence intensity (MFI) of propidium iodide staining and (E) DNA damage assessed by MFI of pH2AX staining in cells exposed to WS and NS particles or soluble U (U aq). Data are expressed as mean ± SD of triplicate samples per treatment. * Statistically significant difference in a one-way ANOVA followed by Dunnett's t-test compared to the untreated control group ($p < 0.05$).

with the cellular components rather than extracellular release/leakage of dissolved U in the cell culture medium. Distinct behavior was reported for other dissolved metal forms (e.g., silver, zinc, and copper) in the induction of cellular toxicity.[36−38] The cytotoxicity and the interaction of U ions with cellular components are not well understood with different behaviors reported depending on the cell type investigated[39] and the route of exposure.[40] For instance, Bolt et al. reported a limited U accumulation in lymphoid tissues following ingestion of soluble U by mice.[41] A recent study noted U accumulation in Jurkat cells; however, accumulation did not induce cytotoxic effects.[39] Medina et al. reported significant immunotoxicity in the GI tract following chronic exposure to drinking water containing soluble U.[42] In vitro studies on soluble U exposure in macrophages showed a significant decrease in cell viability[43] and an induction of inflammatory responses (TNF-α secretion and MAPK activation).[44] Only a few studies have investigated the toxicity of U as particulates. In vivo studies show that exposure to U-oxide particulates induces DNA strand breaks in bronchoalveolar lavage cells, increases lung inflammatory cytokine expression, and enhances the production of hydroperoxides in the lungs.[45] However, in that study, the cellular interactions and uptake of U as particulate were still underestimated and the toxicity of insoluble U particles was mainly attributed to U radiotoxicity.[45] Evaluating the interactions of metals (as particulate or dissolved forms) with cells is important in understanding the mechanisms underlying various disease states.

Genotoxicity in Cells Exposed to C-Rich U-Bearing Particles. The genotoxic activity of C-rich U-bearing particles was assessed by measuring the relative fluorescence intensity of pH2AX in A549 cells post 24 h incubation with the C-rich U-bearing particles or soluble U at 100 and 445 μM U concentrations (Figure 2E). The phosphorylation of histone H2AX represents a sensitive molecular marker for DNA double-strand breaks and allows the detection of genotoxicity in the U-treated cells. Results indicated a significant U-dose-dependent increase ($p < 0.05$) in pH2AX in cells treated with WS particles. However, no significant increase was observed in cells exposed to soluble U or to NS particles at the same equivalent molar concentrations of U.

Both the results of DNA damage and the cell viability tests confirm the high sensitivity of A549 cells when exposed to WS particles compared to soluble U. These findings are consistent with previous studies reporting a negligible induction of genotoxic effects in the presence of soluble U.[39] The distinct genotoxic responses between WS and NS particles could be

https://doi.org/10.1021/acs.est.1c01205
Environ. Sci. Technol. 2021, 55, 9949−9957

related to the difference in their size distribution. It should be noted that the WS treatment contains a mixture of nanometric (<200 nm) and micrometric (1−10 μm) particles (Figure 1C), both of which can potentially have an impact on the uptake and toxicity of particles. Hetland et al. noticed that coarse size fractions of PM_{10} with a higher metal content induced an increase in inflammatory and toxic reactions in lung cells compared to smaller fractions with a lower metal content.[46] Several other studies also report that coarse PM (2.5−10 μm) can be more toxic than fine PM due to its chemical composition and interactions with the cell membrane.[47,48]

Intracellular Uptake of C-Rich U-Bearing Particles in A549 Cells. The cellular uptake of U was investigated following treatment of A549 cells with soluble U and with WS and NS particles at concentrations of 10 and 100 μM U. Significant U uptake ($p < 0.05$) in a U-dose-dependent manner was observed in cells treated with WS and NS particles (Figure 3). These U concentrations are equivalent to 3.2−32 μg of particles per mL for the WS particles and 4.5−45 μg of particles per mL for the NS particles. The uptake of U was observed to be 2.7 to 5 times higher in cells treated with WS particles in comparison to those treated with NS particles (Figure 3). In line with previous results, no measurable uptake of soluble U (U aq) was detected (Figure 3). After 30 min of exposure, 0.15 and 1.74 μg of U were measured in cells exposed to WS particles at 10 and 100 μM U concentrations, respectively. After 24 h exposure, the measured mass of U in cells treated with WS particles at 10 and 100 μM U concentrations increased to 0.9 and 4.7 μg of U, respectively. These results suggest that C-rich U-bearing particles, especially WS particles, can interact with the cells and contribute to the intracellular accumulation of U. To verify this hypothesis, electron microscopy studies were performed to evaluate the uptake potential of particles (Figure 4).

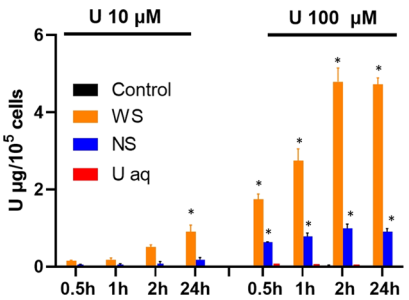

Figure 3. Uranium intracellular accumulation in A549 cells measured by ICP-MS at different time points following incubation with WS and NS groups of C-rich U-bearing particles or soluble U (U aq) at equivalent molar U concentrations of 10 and 100 μM. Data are expressed as mean ± SD of triplicate samples per treatment group. *Statistically significant difference in a one-way ANOVA followed by Dunnett's t-test compared to untreated (control) cells ($p < 0.05$).

The translocation of C-rich U-bearing particles was confirmed for both WS and NS exposures by TEM-EDS analysis, post 24 h incubation of cells to a mass of particles equivalent to 100 μM U (Figure 4). Unlike soluble U, C-rich U-bearing particles were found to interact with the cell membrane, translocate into the cell, and accumulate in the cytoplasm (Figure 4A−K). In cells exposed to WS, some large clusters of C-rich U-bearing particles were observed in large vesicles (~2.5 μm), suggesting that the cells had engulfed large aggregates, possibly by macropinocytosis (Figure 4A−D).

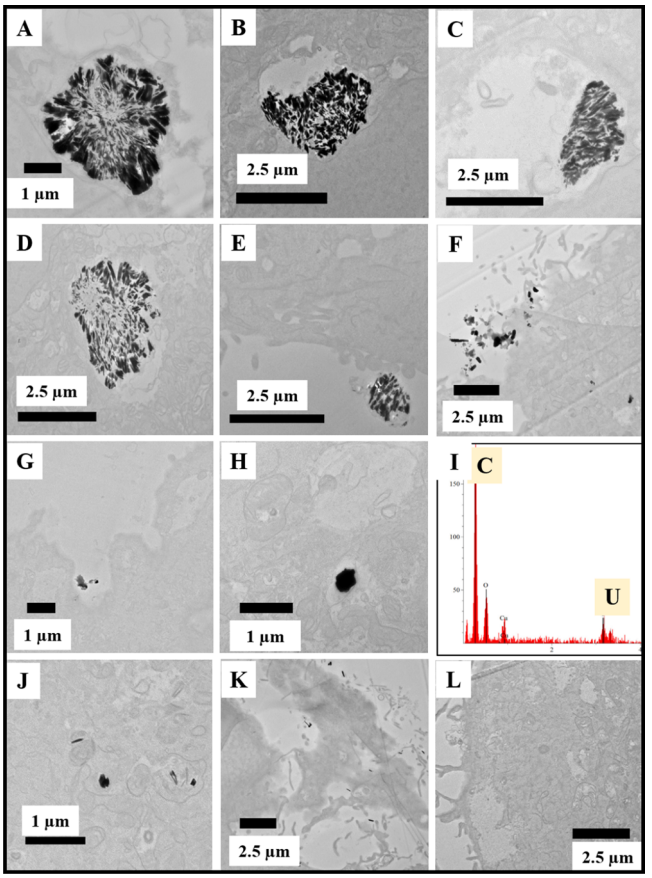

Figure 4. TEM images of A549 cells post 24 h exposure to (A−H) WS particles, (J−K) NS particles and (L) soluble U. (I) Example of the EDS spectrum showing U and C in the detected particles in the cells.

However, in the case of cells exposed to NS, particles were either found dispersed outside the cells, interacting with the membrane, or accumulated separately in the cytoplasm, suggesting uptake possibly through endocytic processes (Figure 4J,K). It should be noted that we also observed in cells exposed to WS some small vesicles and particles entering the cell, as in the case of cells treated with NS (Figure 4G,H). The clusters observed in the WS-exposed cells consist of particles with various sizes assembled in large vesicles, where nanometric particles were found surrounded by their micrometric counterparts (Figure 4A−D). These observations suggest that particles with heterogeneous sizes enhanced the formation of clusters and the aggregation of nanometric particles outside the cells. These interactions may increase the binding affinity with the cell membrane and ultimately induce endocytosis, possibly via macropinocytosis. Figure 4E,F shows examples of particle clusters from the WS-exposed cells containing both micrometric and nanometric particles near the membrane on the outside of the cell. This uptake process has been described as an important nonspecific pathway of particles larger than 400 nm following the membrane extension and formation of large vesicles (with sizes between 0.2 and 5 μm) that entrap extracellular fluid containing the particles.[49] A549 cells were reported in previous studies to take up distinct organic (i.e., C nanoparticles) or metal oxide particles (i.e., silica nanoparticles) through macropinocytosis.[50,51]

The large intracellular accumulation of WS particle clusters confirms their engulfment by epithelial cells. These observa-

https://doi.org/10.1021/acs.est.1c01205
Environ. Sci. Technol. 2021, 55, 9949−9957

tions are in line with our quantitative analysis and with the cyto- and genotoxicity assays, showing a significant accumulation of U and significant toxicity in A549 cells treated with WS particles (compared to those treated with NS particles and soluble U). It is known that intracellular uptake represents an important process determining the reactions of particles with cells.[52−54] Previous studies show that metal particulates can be taken up by cells, facilitate metal intracellular incorporation, and promote metal interactions with proteins, organelles, and nuclear DNA.[52,55] For example, Zhao et al. found that silver particles (<3.5 μm) have an essential role in the translocation of silver to the cell interior and in the induction of toxicity.[55] The intracellular-oriented cytotoxicity of WS particles was confirmed after incubating the particles with nonphagocytic RBCs at U concentrations ranging from 1.11 to 445 μM (Figure S5).[56] Negligible hemolytic activities were obtained even after 24 h incubation with WS particles and with soluble U (Figure S5). However, NS exposure resulted in up to 15% hemolysis after 24 h incubation at 445 μM U concentration (Figure S5), suggesting that NS particles can induce membrane damage over time. The hemolysis results show that NS particles cause a higher membrane disruption than WS (Figure S5) and therefore explain the somehow close cell toxicity data between NS and WS particles (Figure 1A) despite the difference in U cellular uptake. However, WS particles are likely to be less interactive with the surface of the cells and can induce a significant higher DNA damage than NS accompanied (Figure 1E) with a higher intracellular particle uptake and U accumulation (Figures 3 and 4).

Environmental Implications. In this study, we found that different size ranges of C-rich U-bearing particles (<0.2−10 μm) induce significant levels of DNA damage and cell death. The large intracellularly accumulated clusters are composed of both nanometric (<200 nm) and micrometric (<0.9 μm) particles. Particulate U, rather than soluble U, causes U toxicity in lung epithelial cells. Our TEM observations suggest that the micrometric particles in the WS treatment play a role in the cellular uptake of nanometric particles by creating large aggregates. This hypothesis is reinforced by the absence of any detected vesicles with only nanometric particles in the cells. Such phenomena could have important implications for mine site-derived PM, which represents respirable particles with a wide size distribution.[57,58] Further work should focus on the relationship between the physicochemical interactions of nano- and micrometric PM with their cellular uptake and toxicity, as both sizes are environmentally relevant. Additionally, the numerous mineralogical forms of U and co-occurring metals and metalloids (e.g., V, arsenic (As), and copper) may further influence toxicity. Naturally occurring U-containing minerals differ chemically and structurally from the synthesized PM used in the present study. Therefore, further studies are needed to understand how nanometer-sized PM and micrometer-sized PM of minerals such as carnotite, coffinite, or tyuyamunite promote toxic cellular responses through dissolution of metal ions or surface chemical interactions with biomolecules.

Inhalation exposure to even relatively small quantities of mine site-derived PM is of great concern given that high U (or other co-occurring metals) concentrations can be present in the fine-grained particles.[59] Our results show that even a low mass concentration of 4.5 μg mL^{-1} for both the wide and narrow size particle distributions induces 50% cell death after 48 h exposure. This can be related to the concentrated mass of U in the particles translocated into the cells. These findings are of great importance to semi-arid areas where eolian processes facilitate the frequent transport of U-containing PM at a local and regional scale.[3,8,9] In this study, we focused on C-rich U-bearing particles (synthesized as uranyl citrate) as an environmentally relevant model of C-encapsulated U-phases.[13,14] This approach facilitated the identification of key components contributing to the toxicity of PM with a complex chemical composition.[60] Future studies should investigate the toxic effects of other metal particulates and chemical phases. For example, the toxic effect of V and As co-occurring in mineral mixtures with U needs to be further studied. The solubility of U in PM was presented in the literature as the determining factor of U toxicity in the respiratory system.[3,16] In our study, we detected that U in the solid particulate form is more toxic than the same concentration of soluble U ions. Our results show that the toxicity of C-rich U-bearing particles is directly related to the particles themselves and to their ability to translocate and accumulate inside the cell. Further research is needed to understand the intracellular mechanisms of U particulate toxicity and determine if dissolved U is delivered by the particles to critical receptors in the cell. This research could inform future efforts toward regulations for inhalation exposure pathways and brings up the questions regarding the toxicity of the particulate form of metals following inhalation, ingestion, or skin exposure.

■ ASSOCIATED CONTENT

Supporting Information

The Supporting Information is available free of charge at https://pubs.acs.org/doi/10.1021/acs.est.1c01205.

Additional materials and methods, concentrations of NS particles and WS particles (Tables S1 and S2), and SEM images and corresponding EDS spectra, stability test, cell viability assay, and hemolysis assay (Figures S1 to S5) (PDF)

■ AUTHOR INFORMATION

Corresponding Author

Eliane El Hayek − *Department of Chemistry and Chemical Biology, MSC03 2060, University of New Mexico, Albuquerque, New Mexico 87131, United States; Department of Pharmaceutical Sciences, MSC09 5360, University of New Mexico, College of Pharmacy, Albuquerque, New Mexico 87131, United States;* orcid.org/0000-0003-1129-2419; Phone: (001) (505) 582-1362; Email: eelhayek@salud.unm.edu

Authors

Sebastian Medina − *Department of Pharmaceutical Sciences, MSC09 5360, University of New Mexico, College of Pharmacy, Albuquerque, New Mexico 87131, United States; Department of Biology, New Mexico Highlands University, Las Vegas, New Mexico 87701, United States*

Jimin Guo − *Department of Chemical and Biological Engineering, MSC01 1120 and Department of Internal Medicine, Molecular Medicine, MSC08 4720, University of New Mexico, Albuquerque, New Mexico 87131, United States*

Achraf Noureddine − *Department of Chemical and Biological Engineering, MSC01 1120, University of New Mexico,*

https://doi.org/10.1021/acs.est.1c01205
Environ. Sci. Technol. 2021, 55, 9949−9957

Albuquerque, New Mexico 87131, United States; orcid.org/0000-0001-9530-5963

Katherine E. Zychowski − *Department of Biobehavioral Health and Data Sciences, MSC09 5350, University of New Mexico College of Nursing, Albuquerque, New Mexico 87106, United States*

Russell Hunter − *Department of Pharmaceutical Sciences, MSC09 5360, University of New Mexico, College of Pharmacy, Albuquerque, New Mexico 87131, United States*

Carmen A. Velasco − *Department of Civil Engineering, MSC01 1070, University of New Mexico, Albuquerque, New Mexico 87131, United States; Chemical Engineering Faculty, Central University of Ecuador, Ciudad Universitaria, Quito 170129, Ecuador*

Marco Wiesse − *Department of Civil Engineering, MSC01 1070, University of New Mexico, Albuquerque, New Mexico 87131, United States*

Angelea Maestas-Olguin − *Department of Chemical and Biological Engineering, MSC01 1120, University of New Mexico, Albuquerque, New Mexico 87131, United States*

C. Jeffrey Brinker − *Department of Chemical and Biological Engineering, MSC01 1120, University of New Mexico, Albuquerque, New Mexico 87131, United States;* orcid.org/0000-0002-7145-9324

Adrian Brearley − *Department of Earth and Planetary Sciences, MSC03 2040, University of New Mexico, Albuquerque, New Mexico 87131, United States*

Michael Spilde − *Department of Earth and Planetary Sciences, MSC03 2040, University of New Mexico, Albuquerque, New Mexico 87131, United States*

Tamara Howard − *Department of Cell Biology and Physiology, MSC08 4750, University of New Mexico, Albuquerque, New Mexico 87131, United States*

Fredine T. Lauer − *Department of Pharmaceutical Sciences, MSC09 5360, University of New Mexico, College of Pharmacy, Albuquerque, New Mexico 87131, United States*

Guy Herbert − *Department of Pharmaceutical Sciences, MSC09 5360, University of New Mexico, College of Pharmacy, Albuquerque, New Mexico 87131, United States*

Abdul Mehdi Ali − *Department of Earth and Planetary Sciences, MSC03 2040, University of New Mexico, Albuquerque, New Mexico 87131, United States*

Scott Burchiel − *Department of Pharmaceutical Sciences, MSC09 5360, University of New Mexico, College of Pharmacy, Albuquerque, New Mexico 87131, United States*

Matthew J. Campen − *Department of Pharmaceutical Sciences, MSC09 5360, University of New Mexico, College of Pharmacy, Albuquerque, New Mexico 87131, United States*

José M. Cerrato − *Department of Civil Engineering, MSC01 1070, University of New Mexico, Albuquerque, New Mexico 87131, United States;* orcid.org/0000-0002-2473-6376

Complete contact information is available at: https://pubs.acs.org/10.1021/acs.est.1c01205

Notes

The authors declare no competing financial interest.

■ ACKNOWLEDGMENTS

Funding for this research was provided by the National Science Foundation (CAREER 1652619 and CREST 1345169), the National Institute of Environmental Health Sciences Superfund Research Program (P42 ES025589), R01 ES026673, R00 ES029104, and R01CA226537-01. Any opinions, findings, and conclusions or recommendations expressed in this publication are those of the author(s) and do not necessarily reflect the views of the National Science Foundation. Electron microprobe analysis and scanning transmission electron microscopy were performed at the Electron Microbeam Analysis Facility, Department of Earth and Planetary Sciences and Institute of Meteoritics, University of New Mexico, a facility supported by the State of New Mexico, NASA, and the National Science Foundation. TEM images were also generated at the HSC-Electron Microscopy Facility, supported by the University of New Mexico Health Sciences Center. E.E.H. thanks M.M.N.N. for the support along the experimental work.

■ REFERENCES

(1) Shiraiwa, M.; Ueda, K.; Pozzer, A.; Lammel, G.; Kampf, C. J.; Fushimi, A.; Enami, S.; Arangio, A. M.; Fröhlich-Nowoisky, J.; Fujitani, Y.; Furuyama, A.; Lakey, P.; Lelieveld, J.; Lucas, K.; Morino, Y.; Pöschl, U.; Takahama, S.; Takami, A.; Tong, H.; Weber, B.; Yoshino, A.; Sato, K. Aerosol Health Effects from Molecular to Global Scales. *Environ. Sci. Technol.* **2017**, *51*, 13545−13567.

(2) Zychowski, K. E.; Kodali, V.; Harmon, M.; Tyler, C. R.; Sanchez, B.; Ordonez Suarez, Y.; Herbert, G.; Wheeler, A.; Avasarala, S.; Cerrato, J. M.; Kunda, N. K.; Muttil, P.; Shuey, C.; Brearley, A.; Ali, A. M.; Lin, Y.; Shoeb, M.; Erdely, A.; Campen, M. J. Respirable Uranyl-Vanadate-Containing Particulate Matter Derived from a Legacy Uranium Mine Site Exhibits Potentiated Cardiopulmonary Toxicity. *Toxicol. Sci.* **2018**, *164*, 101−114.

(3) Hettiarachchi, E.; Paul, S.; Cadol, D.; Frey, B.; Rubasinghege, G. Mineralogy Controlled Dissolution of Uranium from Airborne Dust in Simulated Lung Fluids (SLFs) and Possible Health Implications. *Environ. Sci. Technol. Lett.* **2019**, *6*, 62−67.

(4) Zychowski, K. E.; Wheeler, A.; Sanchez, B.; Harmon, M.; Steadman Tyler, C. R.; Herbert, G.; Lucas, S. N.; Ali, A. M.; Avasarala, S.; Kunda, N.; Robinson, P.; Muttil, P.; Cerrato, J. M.; Bleske, B.; Smirnova, O.; Campen, M. J. Toxic Effects of Particulate Matter Derived from Dust Samples near the Dzhidinski Ore Processing Mill, Eastern Siberia, Russia. *Cardiovasc. Toxicol.* **2019**, *19*, 401−411.

(5) Lewis, J.; Hoover, J.; MacKenzie, D. Mining and Environmental Health Disparities in Native American Communities. *Curr. Environ. Health Rep.* **2017**, *4*, 130−141.

(6) Hund, L.; Bedrick, E. J.; Miller, C.; Huerta, G.; Nez, T.; Ramone, S.; Shuey, C.; Cajero, M.; Lewis, J. A Bayesian Framework for Estimating Disease Risk Due to Exposure to Uranium Mine and Mill Waste on the Navajo Nation. *J. R. Stat. Soc. Ser. A* **2015**, *178*, 1069−1091.

(7) Harmon, M. E.; Lewis, J.; Miller, C.; Hoover, J.; Ali, A. S.; Shuey, C.; Cajero, M.; Lucas, S.; Zychowski, K.; Pacheco, B.; Erdei, E.; Ramone, S.; Nez, T.; Gonzales, M.; Campen, M. J. Residential Proximity to Abandoned Uranium Mines and Serum Inflammatory Potential in Chronically Exposed Navajo Communities. *J. Expo. Sci. Environ. Epidemiol.* **2017**, *27*, 365−371.

(8) Gil-Loaiza, J.; Field, J. P.; White, S. A.; Csavina, J.; Felix, O.; Betterton, E. A.; Sáez, A. E.; Maier, R. M. Phytoremediation Reduces Dust Emissions from Metal(Loid)-Contaminated Mine Tailings. *Environ. Sci. Technol.* **2018**, *52*, 5851−5858.

(9) Brown, R. D. Geochemistry and Transport of Uranium-Bearing Dust at Jackpile Mine, Laguna, New Mexico, Master thesis, New Mexico Institute of Mining and Technology, 2017.

(10) Avasarala, S.; Brearley, A. J.; Spilde, M.; Peterson, E.; Jiang, Y. B.; Benavidez, A.; Cerrato, J. M. Crystal Chemistry of Carnotite in Abandoned Mine Wastes. *Minerals* **2020**, *10*, 883.

(11) Deditius, A. P.; Utsunomiya, S.; Ewing, R. C. The Chemical Stability of Coffinite, USiO4·nH2O; 0 < n < 2, Associated with Organic Matter: A Case Study from Grants Uranium Region, New Mexico, USA. *Chem. Geol.* **2008**, *251*, 33−49.

(12) Blake, J. M.; De Vore, C. L.; Avasarala, S.; Ali, A.-M.; Roldan, C.; Bowers, F.; Spilde, M. N.; Artyushkova, K.; Kirk, M. F.; Peterson, E.; Rodriguez-Freire, L.; Cerrato, J. M. Uranium Mobility and Accumulation along the Rio Paguate, Jackpile Mine in Laguna Pueblo, New Mexico. *Environ. Sci. Process. Impacts* **2017**, *19*, 605−621.
(13) Velasco, C. A.; Artyushkova, K.; Ali, A. S.; Osburn, C. L.; Gonzalez-Estrella, J.; Lezama-Pacheco, J. S.; Cabaniss, S. E.; Cerrato, J. M. Organic Functional Group Chemistry in Mineralized Deposits Containing U(IV) and U(VI) from the Jackpile Mine in New Mexico. *Environ. Sci. Technol.* **2019**, *53*, 5758−5767.
(14) Avasarala, S.; Torres, C.; Ali, A. M. S.; Thomson, B. M.; Spilde, M. N.; Peterson, E. J.; Artyushkova, K.; Dobrica, E.; Lezama-Pacheco, J. S.; Cerrato, J. M. Effect of Bicarbonate and Oxidizing Conditions on U(IV) and U(VI) Reactivity in Mineralized Deposits of New Mexico. *Chem. Geol.* **2019**, *524*, 345−355.
(15) Asic, A.; Kurtovic-Kozaric, A.; Besic, L.; Mehinovic, L.; Hasic, A.; Kozaric, M.; Hukic, M.; Marjanovic, D. Chemical Toxicity and Radioactivity of Depleted Uranium: The Evidence from in Vivo and in Vitro Studies. *Environ. Res.* **2017**, *156*, 665−673.
(16) Monleau, M.; de Méo, M.; Frelon, S.; Paquet, F.; Donnadieu-Claraz, M.; Duménil, G.; Chazel, V. Distribution and Genotoxic Effects after Successive Exposure to Different Uranium Oxide Particles Inhaled by Rats. *Inhalation Toxicol.* **2006**, *18*, 885−894.
(17) Wilson, A.; Velasco, C. A.; Herbert, G. W.; Lucas, S. N.; Sanchez, B. N.; Cerrato, J. M.; Spilde, M.; Li, Q. Z.; Campen, M. J.; Zychowski, K. E. Mine-Site Derived Particulate Matter Exposure Exacerbates Neurological and Pulmonary Inflammatory Outcomes in an Autoimmune Mouse Model. *J. Toxicol. Environ. Health A* **2021**, *84*, 503−517.
(18) Yellowhair, M.; Romanotto, M. R.; Stearns, D. M.; Clark Lantz, R. Uranyl Acetate Induced DNA Single Strand Breaks and AP Sites in Chinese Hamster Ovary Cells. *Toxicol. Appl. Pharmacol.* **2018**, *349*, 29−38.
(19) Zhang, Q.; Pardo, M.; Rudich, Y.; Kaplan-Ashiri, I.; Wong, J. P. S.; Davis, A. Y.; Black, M. S.; Weber, R. J. Chemical Composition and Toxicity of Particles Emitted from a Consumer-Level 3D Printer Using Various Materials. *Environ. Sci. Technol.* **2019**, *53*, 12054−12061.
(20) Jin, L.; Xie, J.; Wong, C. K. C.; Chan, S. K. Y.; Abbaszade, G.; Schnelle-Kreis, J.; Zimmermann, R.; Li, J.; Zhang, G.; Fu, P.; Li, X. Contributions of City-Specific Fine Particulate Matter ($PM_{2.5}$) to Differential in Vitro Oxidative Stress and Toxicity Implications between Beijing and Guangzhou of China. *Environ. Sci. Technol.* **2019**, *53*, 2881−2891.
(21) Saunders, J. A.; Pivetz, B. E.; Voorhies, N.; Wilkin, R. T. Potential Aquifer Vulnerability in Regions Down-Gradient from Uranium in Situ Recovery (ISR) Sites. *J. Environ. Manage.* **2016**, *183*, 67−83.
(22) Ruiz, O.; Thomson, B. M.; Cerrato, J. M. Investigation of in Situ Leach (ISL) Mining of Uranium in New Mexico and Post-Mining Reclamation. *N. M. Geol.* **2016**, *38*, 77−85.
(23) Gonzalez-Estrella, J.; Meza, I.; Burns, A. J.; Ali, A. M. S.; Lezama-Pacheco, J. S.; Lichtner, P.; Shaikh, N.; Fendorf, S.; Cerrato, J. M. Effect of Bicarbonate, Calcium, and PH on the Reactivity of As(V) and U(VI) Mixtures. *Environ. Sci. Technol.* **2020**, *54*, 3979−3987.
(24) Hansley, P. L.; Spirakis, C. S. Organic Matter Diagenesis as the Key to a Unifying Theory for the Genesis of Tabular Uranium-Vanadium Deposits in the Morrison Formation, Colorado Plateau. *Econ. Geol.* **1992**, *87*, 352−365.
(25) Cumberland, S. A.; Douglas, G.; Grice, K.; Moreau, J. W. Uranium Mobility in Organic Matter-Rich Sediments: A Review of Geological and Geochemical Processes. *Earth-Sci. Rev.* **2016**, *159*, 160−185.
(26) Thuéry, P. Uranyl Ion Complexation by Citric and Tricarballylic Acids : Hydrothermal Synthesis and Structure of Two- and Three-Dimensional Uranium-Organic Frameworks. *Chem. Commun.* **2006**, *8*, 853−855.
(27) Basile, M.; Unruh, D. K.; Gojdas, K.; Flores, E.; Streicher, L.; Forbes, T. Z. Chemical Controls on Uranyl Citrate Speciation and the Self-Assembly of Nanoscale Macrocycles and Sandwich Complexes in Aqueous Solutions. *Chem. Commun.* **2015**, *51*, 5306−5309.
(28) Thuéry, P. Novel Two-Dimensional Uranyl-Organic Assemblages in the Citrate and D(−)-Citramalate Families. *CrystEngComm* **2008**, *10*, 79−85.
(29) Bürglová, K.; Noureddine, A.; Hodačová, J.; Toquer, G.; Cattoën, X.; Wong Chi Man, M. A General Method for Preparing Bridged Organosilanes with Pendant Functional Groups and Functional Mesoporous Organosilicas. *Chemistry* **2014**, *20*, 10371−10382.
(30) Noureddine, A.; Gary-Bobo, M.; Lichon, L.; Garcia, M.; Zink, J. I.; Wong Chi Man, M.; Cattoën, X. Bis-Clickable Mesoporous Silica Nanoparticles: Straightforward Preparation of Light-Actuated Nanomachines for Controlled Drug Delivery with Active Targeting. *Chemistry* **2016**, *22*, 9624−9630.
(31) Chowdhury, P. H.; He, Q.; Carmieli, R.; Li, C.; Rudich, Y.; Pardo, M. Connecting the Oxidative Potential of Secondary Organic Aerosols with Reactive Oxygen Species in Exposed Lung Cells. *Environ. Sci. Technol.* **2019**, *53*, 13949−13958.
(32) Wang, B.; Li, K.; Jin, W.; Lu, Y.; Zhang, Y.; Shen, G.; Wang, R.; Shen, H.; Li, W.; Huang, Y.; Zhang, Y.; Wang, X.; Li, X.; Liu, W.; Cao, H.; Tao, S. Properties and Inflammatory Effects of Various Size Fractions of Ambient Particulate Matter from Beijing on A549 and J774A.1 Cells. *Environ. Sci. Technol.* **2013**, *47*, 10583−10590.
(33) Kim, W.; Jeong, S.-C.; Shin, C.; Song, M.-K.; Cho, Y.; Lim, J.; Gye, M. C.; Ryu, J.-C. A Study of Cytotoxicity and Genotoxicity of Particulate Matter ($PM_{2.5}$) in Human Lung Epithelial Cells (A549). *Mol. Cell. Toxicol.* **2018**, *14*, 163−172.
(34) Liu, S.; Yang, R.; Chen, Y.; Zhao, X.; Chen, S.; Yang, X.; Cheng, Z.; Hu, B.; Liang, X.; Yin, N.; Liu, Q.; Wang, H.; Liu, S.; Faiola, F. Development of Human Lung Induction Models for Air Pollutants' Toxicity Assessment. *Environ. Sci. Technol.* **2021**, *55*, 2440−2451.
(35) Pollard, K. M. Silica, Silicosis, and Autoimmunity. *Front. Immunol.* **2016**, *7*, 97.
(36) Hanagata, N.; Zhuang, F.; Connolly, S.; Li, J.; Ogawa, N.; Xu, M. Molecular Responses of Human Lung Epithelial Cells to the Toxicity of Copper Oxide Nanoparticles Inferred from Whole Genome Expression Analysis. *ACS Nano* **2011**, *5*, 9326−9338.
(37) Hadrup, N.; Sharma, A. K.; Loeschner, K.; Jacobsen, N. R. Pulmonary Toxicity of Silver Vapours, Nanoparticles and Fine Dusts: A Review. *Regul. Toxicol. Pharmacol.* **2020**, *115*, No. 104690.
(38) Olejnik, M.; Kersting, M.; Rosenkranz, N.; Loza, K.; Breisch, M.; Rostek, A.; Prymak, O.; Schürmeyer, L.; Westphal, G.; Köller, M.; Bünger, J.; Epple, M.; Sengstock, C. Cell-Biological Effects of Zinc Oxide Spheres and Rods from the Nano- to the Microscale at Sub-Toxic Levels. *Cell Biol. Toxicol.* **2020**, 1−21.
(39) Dashner-Titus, E. J.; Schilz, J. R.; Simmons, K. A.; Duncan, T. R.; Alvarez, S. C.; Hudson, L. G. Differential Response of Human T-Lymphocytes to Arsenic and Uranium. *Toxicol. Lett.* **2020**, *333*, 269−278.
(40) Brugge, D.; de Lemos, J. L.; Oldmixon, B. Exposure Pathways and Health Effects Associated with Chemical and Radiological Toxicity of Natural Uranium: A Review. *Rev. Environ. Health* **2005**, *20*, 177−193.
(41) Bolt, A. M.; Medina, S.; Lauer, F. T.; Xu, H.; Ali, A.; Liu, J.; Burchiel, S. W. Minimal Uranium Accumulation in Lymphoid Tissues Following an Oral 60-Day Uranyl Acetate Exposure in Male and Female C57BL / 6J Mice. *PLoS One* **2018**, *13*, No. e0205211.
(42) Medina, S.; Lauer, F. T.; Castillo, E. F.; Bolt, A. M.; Ali, A. S.; Liu, K. J.; Burchiel, S. W. Exposures to Uranium and Arsenic Alter Intraepithelial and Innate Immune Cells in the Small Intestine of Male and Female Mice. *Toxicol. Appl. Pharmacol.* **2020**, *403*, No. 115155.
(43) Kalinich, J. F.; Ramakrishnan, N.; Villa, V.; McClain, D. E. Depleted Uranium-Uranyl Chloride Induces Apoptosis in Mouse J774 Macrophages. *Toxicology* **2002**, *179*, 105−114.

https://doi.org/10.1021/acs.est.1c01205
Environ. Sci. Technol. 2021, 55, 9949−9957

(44) Gazin, V.; Kerdine, S.; Grillon, G.; Pallardy, M.; Raoul, H. Uranium Induces TNF Alpha Secretion and MAPK Activation in a Rat Alveolar Macrophage Cell Line. *Toxicol. Appl. Pharmacol.* **2004**, *194*, 49−59.
(45) Monleau, M.; de Méo, M.; Paquet, F.; Chazel, V.; Duménil, G.; Donnadieu-Claraz, M. Genotoxic and Inflammatory Effects of Depleted Uranium Particles Inhaled by Rats. *Toxicol. Sci.* **2006**, *89*, 287−295.
(46) Hetland, R. B.; Cassee, F. R.; Refsnes, M.; Schwarze, P. E.; Låg, M.; Boere, A. J. F.; Dybing, E. Release of Inflammatory Cytokines, Cell Toxicity and Apoptosis in Epithelial Lung Cells after Exposure to Ambient Air Particles of Different Size Fractions. *Toxicol. In Vitro* **2004**, *18*, 203−212.
(47) Monn, C.; Becker, S. Cytotoxicity and Induction of Proinflammatory Cytokines from Human Monocytes Exposed to Fine ($PM_{2.5}$) and Coarse Particles ($PM_{10-2.5}$) in Outdoor and Indoor Air. *Toxicol. Appl. Pharmacol.* **1999**, *155*, 245−252.
(48) Osornio-Vargas, A. R.; Bonner, J. C.; Alfaro-Moreno, E.; Martínez, L.; García-Cuellar, C.; Ponce-de-León Rosales, S.; Miranda, J.; Rosas, I. Proinflammatory and Cytotoxic Effects of Mexico City Air Pollution Particulate Matter in Vitro Are Dependent on Particle Size and Composition. *Environ. Health Perspect.* **2003**, *111*, 1289−1293.
(49) Behzadi, S.; Serpooshan, V.; Tao, W.; Hamaly, M. A.; Mahmoud, Y.; Dreaden, E. C.; Brown, D.; Alkilany, A. M.; Omid, C.; Mahmoudi, M. Cellular Uptake of Nanoparticles: Journey inside the Cell. *Chem. Soc. Rev.* **2018**, *46*, 4218−4244.
(50) Chen, L.; Wang, H.; Li, X.; Nie, C.; Liang, T.; Xie, F.; Liu, K.; Peng, X.; Xie, J. Highly Hydrophilic Carbon Nanoparticles : Uptake Mechanism by Mammalian and Plant Cells. *RSC Adv.* **2018**, *8*, 35246−35256.
(51) Nowak, J. S.; Mehn, D.; Nativo, P.; García, C. P.; Gioria, S.; Ojea-Jiménez, I.; Gilliland, D.; Rossi, F. Silica Nanoparticle Uptake Induces Survival Mechanism in A549 Cells by the Activation of Autophagy but Not Apoptosis. *Toxicol. Lett.* **2014**, *224*, 84−92.
(52) Singh, R. P.; Ramarao, P. Cellular Uptake, Intracellular Trafficking and Cytotoxicity of Silver Nanoparticles. *Toxicol. Lett.* **2012**, *213*, 249−259.
(53) Ahamed, M.; Karns, M.; Goodson, M.; Rowe, J.; Hussain, S. M.; Schlager, J. J.; Hong, Y. DNA Damage Response to Different Surface Chemistry of Silver Nanoparticles in Mammalian Cells. *Toxicol. Appl. Pharmacol.* **2008**, *233*, 404−410.
(54) Wang, Z.; Liu, S.; Ma, J.; Qu, G.; Wang, X.; Yu, S.; He, J.; Liu, J.; Xia, T.; Jiang, G. B. Silver Nanoparticles Induced RNA Polymerasesilver Binding and RNA Transcription Inhibition in Erythroid Progenitor Cells. *ACS Nano* **2013**, *7*, 4171−4186.
(55) Zhao, X.; Ibuki, Y. Evaluating the Toxicity of Silver Nanoparticles by Detecting Phosphorylation of Histone H3 in Combination with Flow Cytometry Side-Scattered Light. *Environ. Sci. Technol.* **2015**, *49*, 5003−5012.
(56) Zhu, W.; Guo, J.; Agola, J. O.; Croissant, J. G.; Wang, Z.; Shang, J.; Coker, E.; Motevalli, B.; Zimpel, A.; Wuttke, S.; Brinker, C. J. Metal-Organic Framework Nanoparticle-Assisted Cryopreservation of Red Blood Cells. *J. Am. Chem. Soc.* **2019**, *141*, 7789−7796.
(57) Gonzales, P.; Felix, O.; Alexander, C.; Lutz, E.; Ela, W.; Eduardo Sáez, A. Laboratory Dust Generation and Size-Dependent Characterization of Metal and Metalloid-Contaminated Mine Tailings Deposits. *J. Hazard. Mater.* **2014**, *280*, 619−626.
(58) Martin, R.; Dowling, K.; Pearce, D. C.; Florentine, S.; Bennett, J. W.; Stopic, A. Size-Dependent Characterisation of Historical Gold Mine Wastes to Examine Human Pathways of Exposure to Arsenic and Other Potentially Toxic Elements. *Environ. Geochem. Health* **2016**, *38*, 1097−1114.
(59) Blake, J. M.; Avasarala, S.; Artyushkova, K.; Ali, A.-M. S.; Brearley, A. J.; Shuey, C.; Robinson, W. P.; Nez, C.; Bill, S.; Lewis, J.; Hirani, C.; Pacheco, J. S. L.; Cerrato, J. M. Elevated Concentrations of U and Co-Occurring Metals in Abandoned Mine Wastes in a Northeastern Arizona Native American Community. *Environ. Sci. Technol.* **2015**, *49*, 8506−8514.
(60) Pan, X.; Yuan, X.; Li, X.; Gao, S.; Sun, H.; Zhou, H.; Hou, L.; Peng, X.; Jiang, Y.; Yan, B. Induction of Inflammatory Responses in Human Bronchial Epithelial Cells by Pb^{2+}-Containing Model $PM_{2.5}$ Particles via Downregulation of a Novel Long Noncoding RNA Lnc-PCK1-2:1. *Environ. Sci. Technol.* **2019**, *53*, 4566−4578.

https://doi.org/10.1021/acs.est.1c01205
Environ. Sci. Technol. 2021, 55, 9949−9957